

ROCK MATRIX AND FRACTURE ANALYSIS OF FLOW IN  
WESTERN TIGHT GAS SANDS

Quarterly Technical Progress Report  
April-June, 1985

N.R. Morrow  
J.S. Ward  
K.R. Brower

New Mexico Petroleum Recovery Research Center  
New Mexico Institute of Mining and Technology  
Socorro, New Mexico

Contributors:

Shirleen Bretz  
Vijaya Dandge  
Mary Graham  
Ingrid Klich

PRRC Report 85-36

Prepared for  
the Department of Energy  
Under Contract No. De-AC21-84MC21179

NOTICE

This report was prepared as an account of work sponsored by an agency of the United States Government. Neither the United States Government nor any agency thereof, nor any of their employees, makes any warranty, express or implied, or assumes any legal liability or responsibility for the accuracy, completeness, or usefulness of any information, apparatus, product, or process disclosed, or represents that its use would not infringe privately owned rights. Reference herein to any specific commercial product, process, or service by trade name, trademark, manufacturer, or otherwise, does not necessarily constitute or imply its endorsement, recommendation, or favoring by the United States Government or any agency thereof. The views and opinions of authors expressed herein do not necessarily state or reflect those of the United States Government or any agency thereof.

## Task 1. Advanced Core Analysis

Advanced core analysis includes measurements on the matrix properties of the rock. Matrix properties are important even in fractured wells since it is these properties which determine the rate of gas flow into the fractures.

Cores are being tested from the fluvial, coastal, and paludal zones of the Mesaverde. At least two cores from each of these zones from all three wells will be analyzed. Properties measured include permeability as a function of confining pressure over the range of 500 to 5000 psi. A minimum of two Klinkenberg permeabilities are being determined from at least five data points. Interpretation includes estimates of pore size from gas slippage. Water adsorption and desorption isotherms will be determined for selected samples with data points being obtained at the following relative humidities: 0, 20, 40, 60, 75, 90, 98, and 100.

Porosity measurements from both thin section examination and volumetric measurements are being made. These results will be compared with the porosities of the cored intervals determined from logs.

### Progress

The Multiwell samples on hand and work in progress and completed for the advanced core analysis task are summarized in Table 1.

Permeability Measurements: Six samples from the fluvial geologic zone have been selected for study, including two samples from each well. The samples chosen are marked with an asterisk in Table 1. Core plugs were cut and oven-dried at 110°C until constant weights were obtained. Gas permeabilities were measured by the method reported previously.<sup>1</sup> Table 2 shows the results of permeability measurements at 5000 and 500 psi confining pressure for first unloading. Crack thickness estimates derived from the slope of permeability vs. confining pressure plots are included in Table 2 as well as the ratio of Klinkenberg permeabilities at 500 and 5000 psi which is an indicator of the severity of pressure sensitivity for these samples.

Adsorption-desorption Isotherms: Cores from the same six fluvial zone samples chosen above for the permeability measurements were cut and dried at 110°C for determination of water desorption and adsorption isotherms. The samples were saturated under vacuum with deaerated distilled water. After complete saturation was attained, cores were introduced into a dessicator with humidity controlled at 98% by a sulfuric acid and water solution. Periodic weighing was used to monitor equilibration at each relative humidity, and samples were moved to chambers of successively lower relative humidity after equilibrium was achieved. The results for water desorption are shown in Fig. 1. The adsorption experiment is still in progress.

Surface Area Measurements: Surface areas have been measured by the BET single point method for the most recently received set of core samples. Results of these measurements are shown in Table 3. Porosities measured by the Boyle's law expansion of helium gas are included in Table 3, as well as the value of the surface area to pore volume ratio calculated from these two measurements.

Comparison of Core Drying Environments: The conditions under which a core is stored and prepared for analysis can have a significant influence on the outcome of subsequent core testing. Drying at high temperature, or even prolonged low temperature drying can dehydrate clay minerals resulting in irreversible structural changes. Pore volume measurements and subsequent saturation calculations also depend on the initial state of the core.

Three of the fluvial zone samples (designated in Table 1 by a dagger symbol) were chosen to investigate the influence of drying procedures on these Multiwell samples. Two additional core plugs were cut from each of these samples. Equilibration in a 45% relative humidity environment at room temperature was substituted for the oven-drying step. One set of core plugs is being used to establish the water desorption-adsorption isotherms. Results are not yet available for these samples. The other set has been used to measure permeabilities as a function of confining pressure (first unloading) for comparison to the samples which were dried in the oven at 110°C.

Fig. 2 shows a significant difference in permeabilities between the oven-dried and unheated, humidified samples of MWX1 22-20. These and subsequent permeabilities are measured first at the highest confining pressure, then at successively lower pressures, with gas pressure of 350 psi for all measurements. The oven-dried sample has higher permeability and lower pressure sensitivity than the unheated sample. Fig. 3 shows similar results for two samples of MWX3 58-14. Following the permeability measurements, the unheated, humidified sample was reequilibrated at a lower relative humidity (20%). Fig. 3 includes permeability results after reequilibration which indicate only a slight increase in permeability after this drying step.

Tests with MWX2 17-22 show the limits of reversibility of the drying process. As shown in Fig. 4, the humidified sample is again less permeable than the oven-dried one. Rehumidifying the oven-dried sample decreases permeability, but not to the level of the core which had never

been heated. To establish whether this effect could be attributed to core treatment rather than preexisting differences between the two core plugs, one further set of tests was performed. The sample which had originally been equilibrated at room temperature and 45% relative humidity was dried in the oven at 110°C. Permeability increased as expected. The sample was then rehumidified and permeability measured a third time. Permeabilities were lower than after the high temperature drying step, but not as low as originally measured for this sample. This incomplete reversibility suggests that structure within the pore space has been changed, probably by dehydration of clay minerals. These results are summarized in Table 4.

## Task 2. Flow Along and Across Fractures and Pore Space Heterogeneities

Sometimes production from low permeability gas sands is much higher than could be expected from the properties of the rock matrix as determined by core analysis. The presence of natural fractures is often cited as a key factor in gas production for both fractured and unfractured wells. Vertical fractures have been found in some of the cores recovered in the Multiwell project. The cores show that by far the majority of fractures become filled with calcite cement.

As part of this project, flow measurements are being made along and across selected fractured samples as a function of overburden pressure for a minimum of five core samples. Comparative measurements will be made on unfractured neighboring zones of a given whole core sample. Permeability measurements will be made at a minimum of four levels of water saturation for each of at least six samples to assess the effect of water content on permeabilities in fractured systems. The effects of chemical treatments on mineralized fractures will be studied to assess whether such treatments lead to permeability enhancement or formation damage.

### Progress

The previous quarterly report described preliminary observations of preferential flow paths revealed by viewing the evolution of gas bubbles flowing from an exposed whole-core rock surface. An apparatus has recently been constructed which is designed to measure the effect of overburden pressure on the rate of gas evolution from these preferential flow channels.

### Task 3. Chemical Alteration

Chemical alteration of various mineralogical components and resultant effects on permeability will be investigated. Experiments will include the use of various reagents, including weak acids (e.g. acetic acid), strong acids (e.g.  $\text{HClO}_4$ ), alkali, and chelating agents (e.g. EDTA). The objective of this work is to determine which features of pore structure determine flow properties and also to explore new possibilities for chemical stimulation of low permeability gas sands.

#### Progress

Preliminary work on the alteration of core properties is presently focussed on changes that can accompany core recovery and drying procedures. This work was described under Task 1.

#### Task 4. Effect of Water on Gas Production

Water is known to modify greatly the flow of gas in tight sand and is a key factor in gas production. Permeability to gas will be measured at various levels of water saturation established by equilibration of core samples in humidity chambers. Electrical resistivity at various levels of water saturations and confining pressures will also be measured. Special attention will be given to water distribution within the rock pore space. Circumstances under which water can act to inhibit gas production and the pressure differences necessary to overcome capillary seals formed by water will also be investigated. Capillary pressure measurements will be made using a high-speed centrifuge.

#### Progress

##### Capillary Pressure Curves from Centrifuge Data: An Update

Capillary pressure curves can be obtained from centrifuge experiments by the method first proposed by Hassler and Brunner.<sup>2</sup> This method requires differentiation of a plot of capillary pressure multiplied by average saturation as a function of the pressure. Graphical methods have been used to differentiate the data obtained for the low permeability Multiwell core samples because preliminary results showed that no simple model would fit both low-speed and high-speed data from the centrifuge.

Experience has since shown that the high-speed data do not fit the Hassler-Brunner model. Slopes of the Hassler plot begin to increase, implying an increasing saturation at the core inlet with increasing rotational speed which is not physically realistic. Consequently, data for speeds greater than about 16,000 RPM are not interpretable by this method. It may therefore be acceptable to use curve-fitting techniques to facilitate analysis of lower-speed centrifuge data.

## Graphical Methods

The Hassler-Brunner analysis results in an approximating equation of the form:

$$S_w(z) = \frac{d(z\bar{S}_w)}{dz} \quad (1)$$

where  $z$  is the capillary pressure at the inlet end of the core.

Fig. 5 illustrates the graphical technique used to interpret data according to the Hassler-Brunner method. Currently three points are measured, points A, B, and C as shown. B is the point of tangency and is the pressure reported. Saturation is calculated from the slope of the line defined by the remaining two points, A and C. Actually, two points would be sufficient to define both pressure and slope as long as one was the point of tangency, but an additional measurement is included which is as far as possible out on the tangent, to minimize the importance of measurement errors when differences are taken to obtain the slope. For purposes of comparison, this will be referred to as Method 1 for the remainder of this report.

Another graphical method, closely related to the first, makes use of plots of average saturation as a function of capillary pressure.<sup>3</sup> Equation (1) is expressed as:

$$S_w = z \frac{d\bar{S}_w}{dz} + \bar{S}_w \quad (2)$$

As shown in Fig. 6, a tangent drawn to a smoothed curve through the data can be extrapolated to  $z=0$  (point A). The inverse of the slope of the tangent is:

$$\frac{d\bar{S}_w}{dz} = (\bar{S}_{wb} - \bar{S}_{wa})/z$$

which, on substitution into Equation 2 gives:

$$S_w = 2\bar{S}_{wb} - \bar{S}_{wa}. \quad (3)$$

Again, two measurements are required. Since the same basic equation (Equation 1) and similar measurements are made, the errors involved in this second method should be comparable to those in Method 1. A comparison of these two methods is included in Fig. 7 for three cases. Differences between results of the two methods may be due to the way smoothed curves are drawn and bias introduced by the appearance of  $z$  in both  $x$  and  $y$  terms for Method 1. Method 3, also shown for these cases, involves curve-fitting as discussed in the next section.

#### Curve-Fitting Method

A reasonable least-squares fit to  $\log P_c$  vs.  $\log \bar{S}_w$  was obtained for nearly all of the Multiwell data. Figs. 8 and 9 show data points and best-fit curves for two brine experiments with Multiwell cores. Fig. 10 shows the same information for decane. Given the experimental scatter, most of the least-squares lines give acceptable and sometimes excellent fits. Correlation coefficients ( $r^2$ ) of less than 0.99 generally point to scatter in the data.

Fig. 10a demonstrates a situation where the data clearly do not fit the model. In this case, the receiving tube filled early in the run. The later data do not accurately reflect pressure-saturation relationships, but rather are limited to the maximum visible tube volume. The poor fit

must be attributed to the quality of the data, not the empirical model equation.

In cases where acceptable fits are obtained, the model equation can be differentiated analytically and  $S_w$  calculated as follows:

$$z = a \overline{S_w}^b$$

where  $a$  and  $b$  are the least-squares fit parameters. Then

$$\overline{S_w} = (z/a)^{1/b}$$

which can be differentiated to give:

$$\frac{d\overline{S_w}}{dz} = a^{-1/b} b^{-1} z^{(1/b - 1)}$$

and substitution into Equation (2) gives:

$$S_w = \overline{S_w} (1 + 1/b). \tag{4}$$

Fig. 7 includes some sample results. The Method 2 curves are closely reproduced in all three cases.

Core B (MWX1 42-25) was included in both runs 1 and 5. Fig. 11 compares the capillary pressure curves obtained in these duplicate experiments by Methods 1 and 3. The capillary pressure curves obtained by Method 3 are much more nearly alike than those from Method 1 suggesting that Method 1 introduces more scatter. Method 3 will be used routinely to process centrifuge data, with computer generated plots used to confirm the validity of the fits obtained. Details of the data processing

procedure are available in PRRC report #85-35. A summary of the best-fit parameters for the Multiwell data obtained so far is presented in Table 5.

## References

1. Morrow, N.R., K.R. Brower, and N.H. Kilmer, "Relationship of Pore Structure to Fluid Behavior in Low Permeability Gas Sands," DOE/BC/10216-14, Oct. 1983.
2. Hassler, G.L. and E. Brunner, "Measurement of Capillary Pressures in Small Core Samples," Trans. AIME 160 (1945), pp. 114-123.
3. Amaefule, J., personal communication (1985).

Table 1

## MULTI-WELL SAMPLES

Well	ID	Depth (ft)	Geologic Zone	Gas Permeability	Relative Permeability	Adsorption-Desorption	Surface Area	Clay Analysis	Pore Cast	Electrical Resistivity	Thin Section
MX-1	3-11	4319.4-4320.4	PAR						X		
MX-1	3-21	4308.3-4309.1	PAR						X		
MX-1	8-16	4548.4-4548.9	FM						X		
MX-1	10-13	4699.7-4700.5	FM *	X		in progress	X	X	X		
MX-1	13-15	4851.0-4851.5	FM								
MX-1	22-20	5357.2-5357.7	FP *†	X		in progress	X	X	X		
MX-1	29-24	5725.7-5726.6	FP						X		
MX-2	17-22	4937.0-4937.8	FM *†	X		in progress	X	X	X		
MX-2	47-34	4195.5-4916.6	FM *	X		in progress	X	X	X		
MX-1	14-24A	4917.9-4918.2	FM						X		
MX-1	14-24B	4918.2-4918.9	FM						X		
MX-3	58-14	4918.1-4918.7	FM *†	X		in progress	X	X			
MX-3	60-19	5726.3-5726.8	FP *	X		in progress	X	X			
MX-3	63-16	5832.1-5832.6	FP								
MX-3	64-29	6464.5-6465.0	CO	X	X	X	X				
MX-3	66-17	6893.4-6893.8	PAL	X	X	X	X				
MX-3	67-16	7096.1-7096.7	PAL	X	X	X	X				
MX-3	67-35	7134.2-7134.6	PAL	X	X	X	X				
MX-3	68-15	7551.2-7551.7	SH								
MX-1	3-25	4330.7-4331.6	PAR	X		X	X				
MX-1	A-CO	6402.1-6402.7	CO								
MX-1	B-CO	6435.3-5436.1	CO				X				
MX-1	C-CO	6502.7-6503.2	CO				X				
MX-1	D-CO	6536.5-6537.1	CO				X				
MX-2	E-CO	6432.6-6433.2	CO				X				
MX-2	F-CO	6452.0-6453.0	CO				X				
MX-2	G-CO	6471.8-6472.3	CO				X				
MX-2	H-CO	6507.4-6508.0	CO				X				
MX-2	I-CO	6537.0-6537.9	CO				X				
MX-2	J-PAL	7119.4-7120.3	PAL				X				
MX-2	K-PAL	7139.2-7139.9	PAL				X				
MX-2	L-PAL	7278.9-7279.7	PAL				X				
MX-3	M-CO	6445.0-6445.8	CO				X				
MX-3	N-CO	6461.1-6461.8	CO				X				

KEY TO GEOLOGIC ZONE: CO = Coastal FM = Fluvial (Meander belts) FP = Fluvial (Point bars) PAR = Paralic  
 FM = Fluvial (Meander belts) PAL = Paludal SH = Shoreline/Marine

\*Fluvial zone samples selected for permeability and water adsorption-desorption measurements.  
 †Samples selected for drying conditions study.

Table 2  
PERMEABILITIES, POROSITIES AND SURFACE AREAS  
OF FLUVIAL ZONE MULTIWELL SAMPLES

Sample	Depth (ft.)	Porosity (%)	Surface Area (m <sup>2</sup> /g)*	Permeability (md) For First Unloading		Calculated Crack Thickness		
				K <sub>∞,500</sub>	K <sub>∞,5000</sub>	500 psi (μm)	5000 psi (μm)	
MMX-1 10-13	4699.7-4700.5	6.15	1.60*	0.0142	0.00102	0.228	0.0575	13.92
MMX-1 22-20	5357.2-5357.7	6.29	1.36	0.00659	0.000405	0.188	0.0507	16.27
MMX-2 47-34	4915.5-4916.6	10.25	1.07	0.0895	0.0234	0.298	0.209	3.82
MMX-2 17-22	4937.0-4937.8	8.85	2.31* 1.44	0.00822	0.00182	0.0991	0.101	4.52
MMX-3 58-14	4918.1-4918.7	7.10	3.24*	0.0288	0.00286	0.462	0.186	10.07
MMX-3 60-19	5726.3-5726.8	9.39	2.62*	0.0443	0.00743	0.327	0.128	5.96

\*Starred measurements are for uncrushed core samples; others are for crushed samples.

Table 3

SURFACE AREAS AND POROSITY MEASUREMENTS FOR  
MULTIWELL SAMPLES RECEIVED MARCH 1985

<u>Well</u>	<u>ID</u>	<u>Depth/Ft.</u>	<u>Surface Area m<sup>2</sup>/g (crushed samples)</u>	<u>Percent Porosity Using Helium Porosimeters</u>	<u>Surface to Volume Ratio (m<sup>2</sup>/cc pore vol.)</u>
MWX-1	B-CO	6435.3-6436.1	1.27	4.99	64.1
MWX-1	C-CO	6502.7-6503.2	2.00	4.05	125.6
MWX-1	D-CO	6536.5-6537.1	1.94	8.04	58.8
MWX-2	E-CO	6432.6-6433.2	2.13	5.53	96.4
MWX-2	F-CO	6452.0-6453.0	1.50	5.88	63.6
MWX-2	G-CO	6471.8-6472.3	1.79	5.28	85.1
MWX-2	H-CO	6507.4-6508.0	1.41	5.93	59.3
MWX-2	I-CO	6537.0-6537.9	1.50	8.06	45.3
MWX-2	J-PAL	7119.4-7120.3	2.15	9.48	54.4
MWX-2	K-PAL	7139.2-7139.9	1.94	7.40	64.3
MWX-2	L-PAL	7278.9-7279.7	1.44	7.03	50.5
MWX-3	M-CO	6445.0-6445.8	3.57	7.01	125.5
MWX-3	N-CO	6461.1-6461.8	3.46	8.33	100.9
MWX-3	R-CO	6511.9-6512.4	3.05	5.13	149.5

Key to ID: CO = Coastal Zone  
PAL = Paludal Zone

Table 4

EFFECT OF DRYING PROCEDURE ON PERMEABILITIES  
OF MULTIWELL FLUVIAL SAMPLES

Sample	Depth (ft.)	Treatment	Porosity (%)	Permeability* ( $\mu$ d)		Estimated Crack Thickness ( $\mu$ m)		$\frac{k_{\infty,500}}{k_{\infty,5000}}$
				$k_{\infty,500}$	$k_{\infty,5000}$	@ 500 psi	@ 5000 psi	
MX1 22-20	5357.2-5357.7	Plug I - oven-dried at 110°C	6.29	6.59	0.405	0.188	0.0507	16.27
		Plug II - 45% rel. humidity	5.07	3.84	0.0855	0.204	0.0455	44.91
MX2 17-22	4937.0-4937.8	Plug I - oven-dried at 110°C	8.85	8.22	1.82	0.0991	0.101	4.52
		Plug I - rehumidified at 45%		6.62	0.709	0.208	0.064	9.34
		Plug II - 45% rel. humidity	7.49	7.28	0.784	0.195	0.0725	9.29
MX3 58-14	4918.1-4918.7	Plug II - oven-dried		11.6	2.36	0.237	0.137	4.92
		Plug II - 45% rel. humidity		10.3	1.03	0.343	0.0796	10.0
		Plug I - oven-dried at 110°C	7.10	28.8	2.86	0.462	0.186	10.07
		Plug II - 45% rel. humidity	5.04	17.9	0.708	0.403	0.078	25.28
		Plug II - 20% rel. humidity		17.9	0.994	0.249	0.0919	18.01

\* First Unloading

Table 5

Summary of Best Fits of Multiwell Data to  
Equations of the Form  $P_c(\text{psi}) = a \times S_w^b$

<u>Core ID</u>	<u>Run #</u>	<u>Fluid*</u>	<u>a</u>	<u>b</u>	<u>r<sup>2</sup></u>
MWX1 42-25 A	1	B	112.82	-4.09	.982
B	1	B	110.22	-4.02	.968
A	3	F	95.97	-4.19	.978
B	4	B	107.17	-3.94	.972
B	5	B	77.56	-4.10	.981
	7	D	24.11	-3.59	.990
	8	D	29.35	-3.64	.990
	10	M	69.18	-2.98	.744
MWX2 51-19 C	1	B	123.20	-3.83	.986
D	1	B	98.41	-3.64	.991
D	3	F	72.89	-3.78	.986
C	4	B	112.52	-4.03	.976
C	5	B	90.94	-3.86	.983
	7	D	23.67	-3.39	.993
	8	D	30.70	-3.34	.991
	10	M	20.69	-4.90	.952
MWX3 64-29 F	1	B	78.39	-4.39	.996
E	1	B	87.44	-4.62	.987
E	3	F	72.16	-4.38	.982
F	4	B	50.45	-4.97	.989
F	5	B	58.12	-4.11	.993
	7	D	18.09	-4.15	.992
	7	D	16.21	-3.89	.993
	8	D	20.63	-4.05	.989
	10	M	21.32	-4.80	.996
MWX3 67-16 AA	2	B	97.02	-4.15	.960
GG	3	F	98.49	-3.54	.989
AA	4	B	97.41	-2.94	.995
AA	5	B	86.01	-3.11	.970
GG	5	B	97.61	-3.02	.993
	8	D	32.92	-3.26	.991
	10	M	43.36	-3.26	.993

\*B = 8% KNO<sub>3</sub> brine

D = n-decane

F = Flo-Back mixture (96 parts 3% KCl, 4 parts methanol with 2% Flo-Back 10)

M = Methanol

Table 5 (continued)

Summary of Best Fits of Multiwell Data to  
Equations of the Form  $P_c(\text{psi}) = a \times S_w^b$

<u>Core ID</u>	<u>Run #</u>	<u>Fluid*</u>	<u>a</u>	<u>b</u>	<u>r<sup>2</sup></u>
MWX3 67-35 FF	2	B	37.76	-4.62	.960
EE	2	B	38.39	-4.74	.959
FF	3	F	45.98	-2.97	.982
EE	4	B	37.63	-3.44	.956
FF	4	B	24.40	-4.07	.934
EE	5	B	43.82	-3.31	.987
	7	D	9.26	-5.33	.738
	8	D	13.09	-4.24	.867
	10	M	11.99	-4.32	.940
	12	D	21.45	-2.75	.98
MWX1 3-25 H	6	F	22.02	-3.52	.994
I	6	B	25.80	-3.41	.986
J	6	B	24.46	-3.93	.993
	9	D	8.59	-4.22	.989**
	10	M	7.47	-4.17	.989
	12	D	9.28	-4.30	.938

\*B = 8% KNO<sub>3</sub> brine

D = n-decane

F = Flo-Back mixture (96 parts 3% KCl, 4 parts methanol with 2% Flo-Back 10)

M = Methanol

\*\*RPM  $\leq$  6000

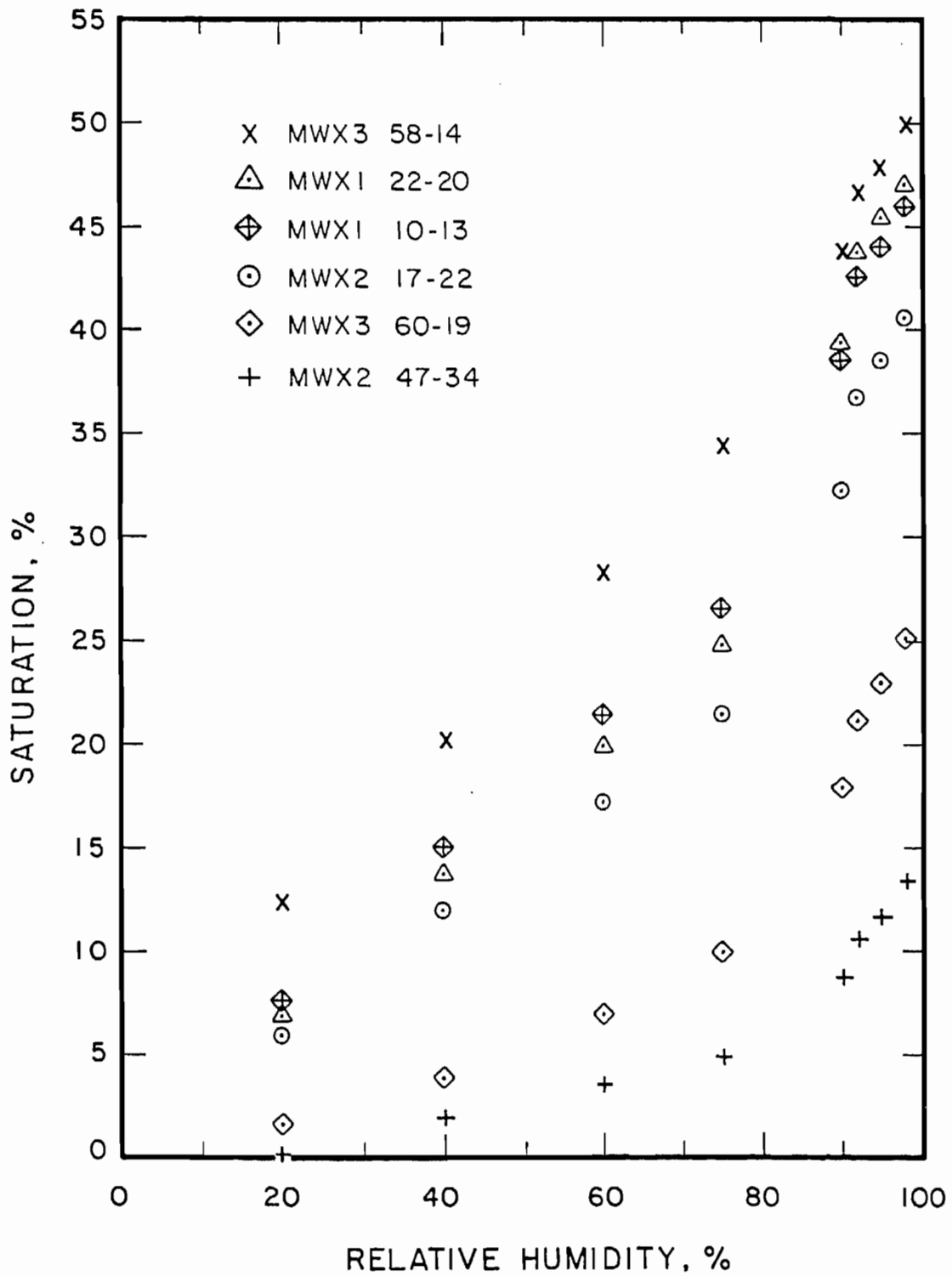


Figure 1. Desorption isotherms for Multiwell Fluvial zone samples.

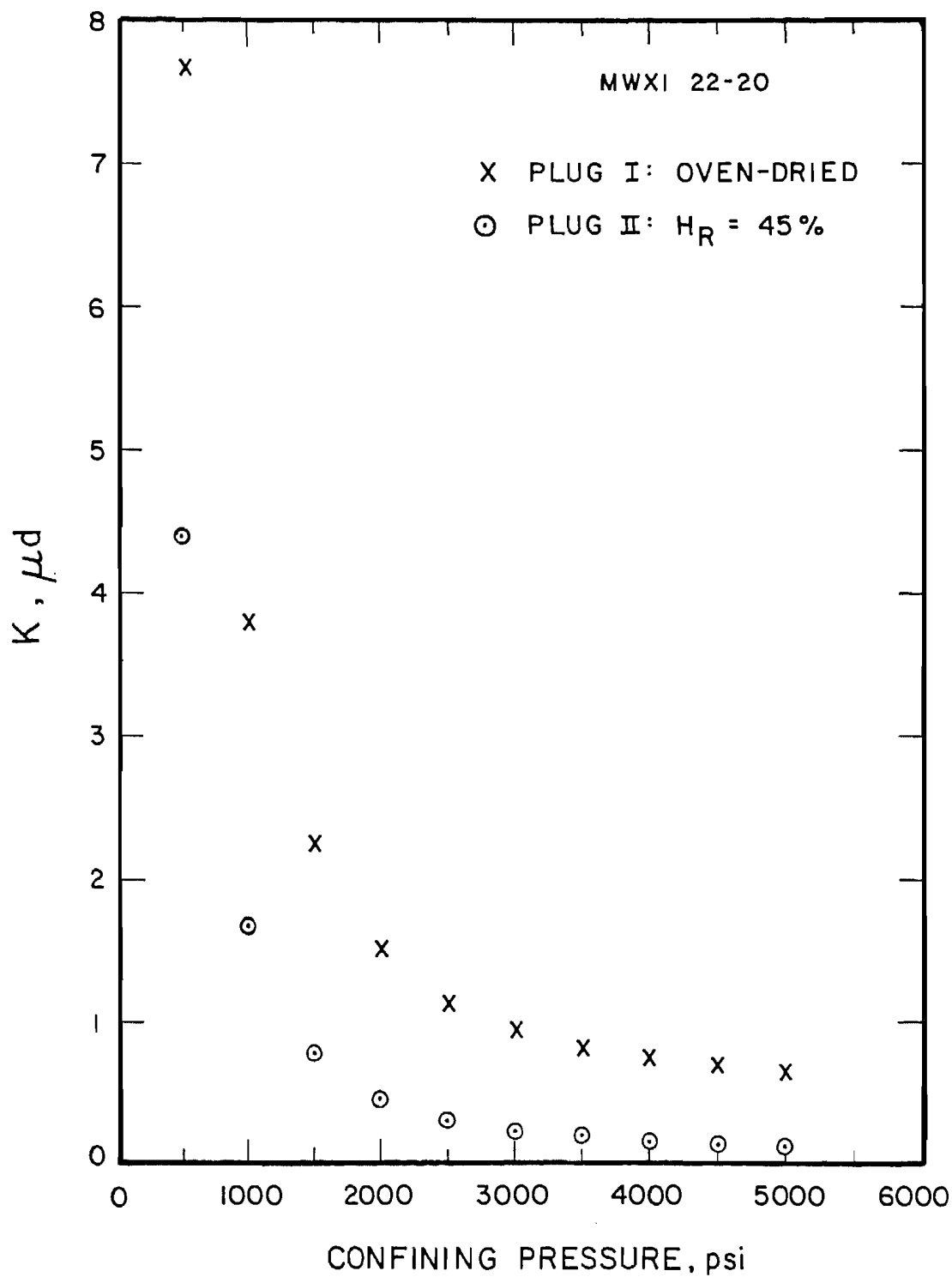


Figure 2. Comparison of MWX1 22-20 gas permeabilities (measured using 350 psi  $N_2$  pressure at successively lower confining pressures) for two sample drying procedures.

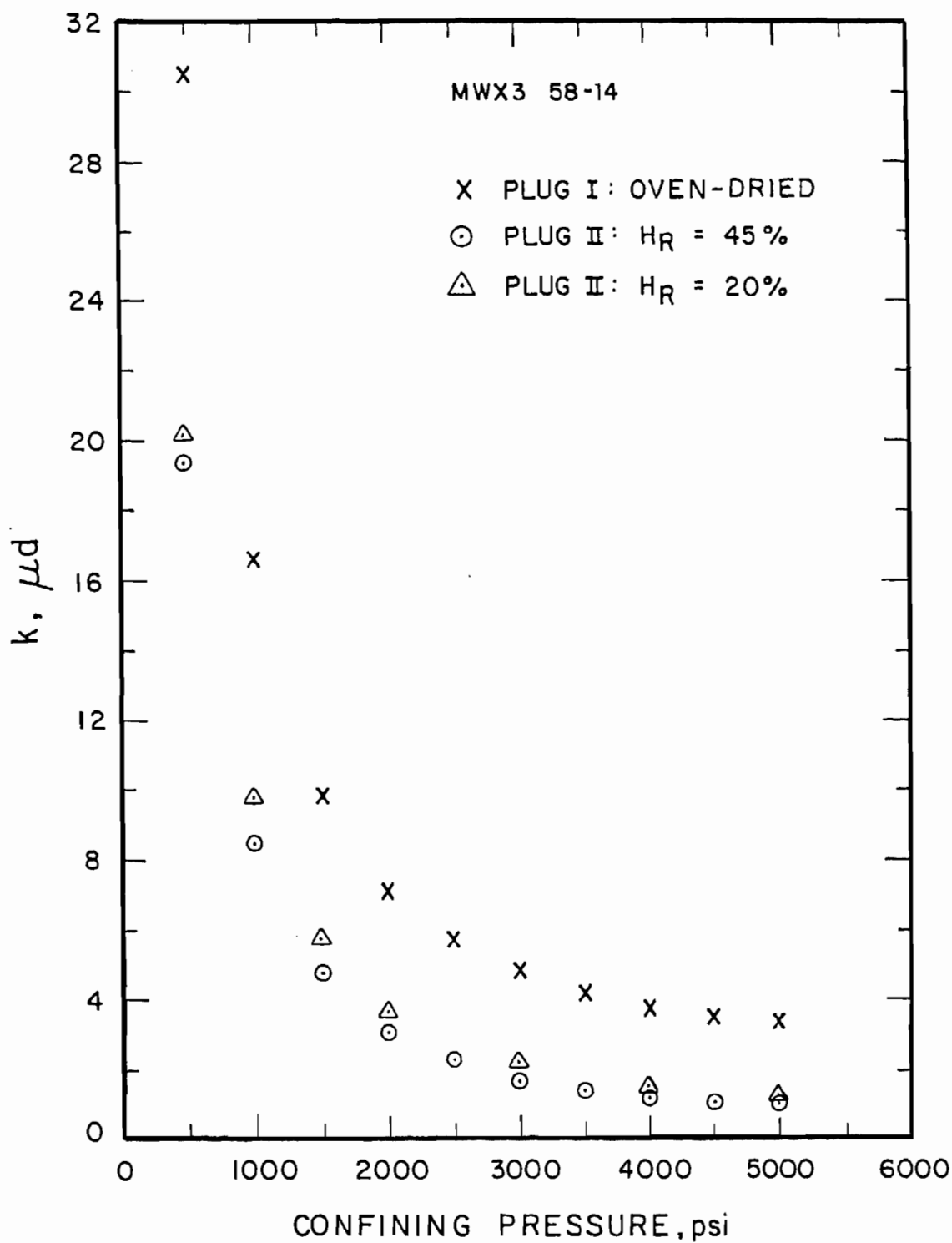


Figure 3. Comparisons of MWX3 58-14 gas permeabilities (measured using 350 psi  $N_2$  pressure at successively lower confining pressures) for oven-dried and humidified core plugs.

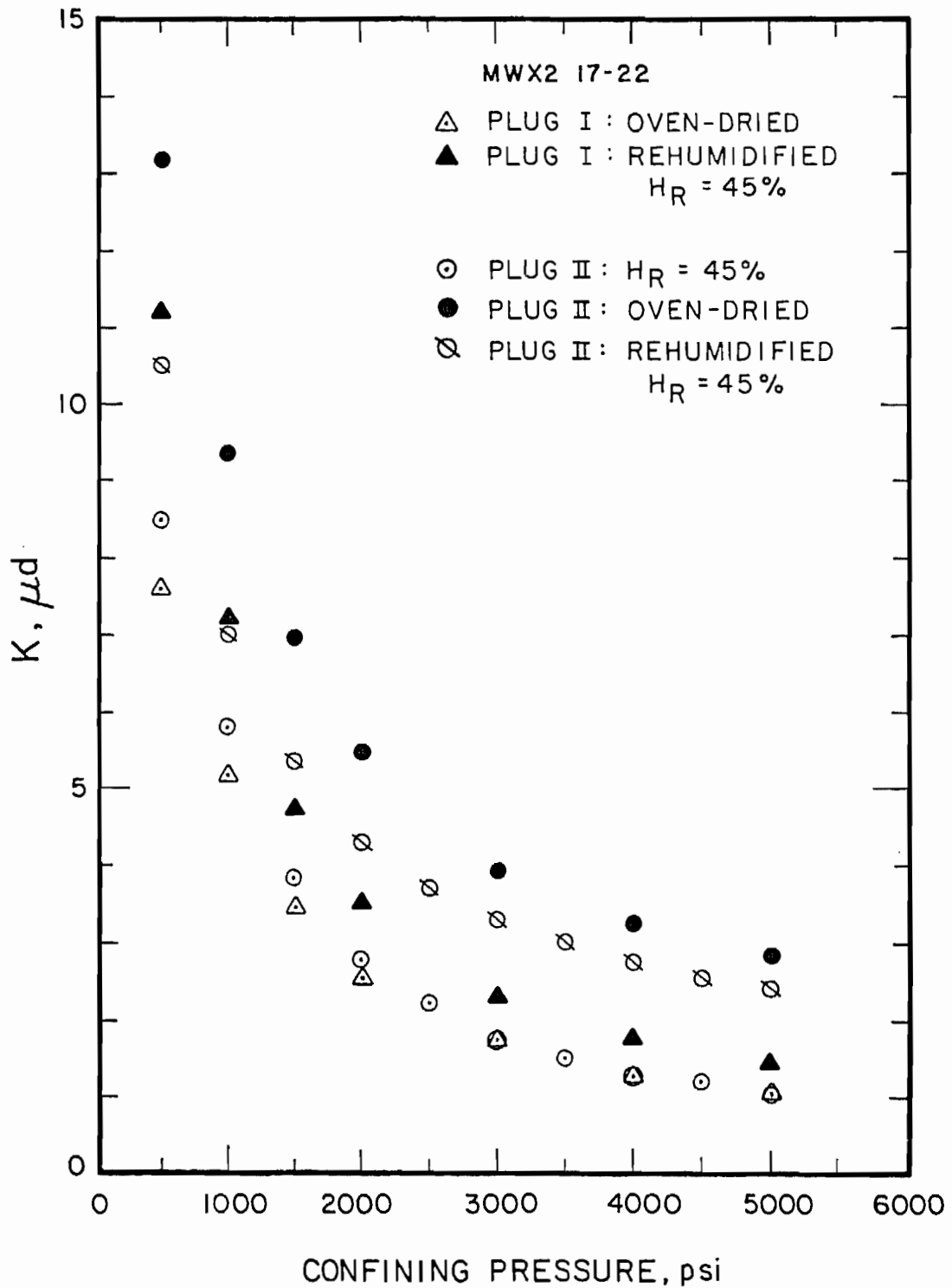


Figure 4. Comparisons of MWX2 17-22 gas permeabilities (measured using 350 psi N<sub>2</sub> pressure at successively lower confining pressures) for two drying techniques in varied sequences.

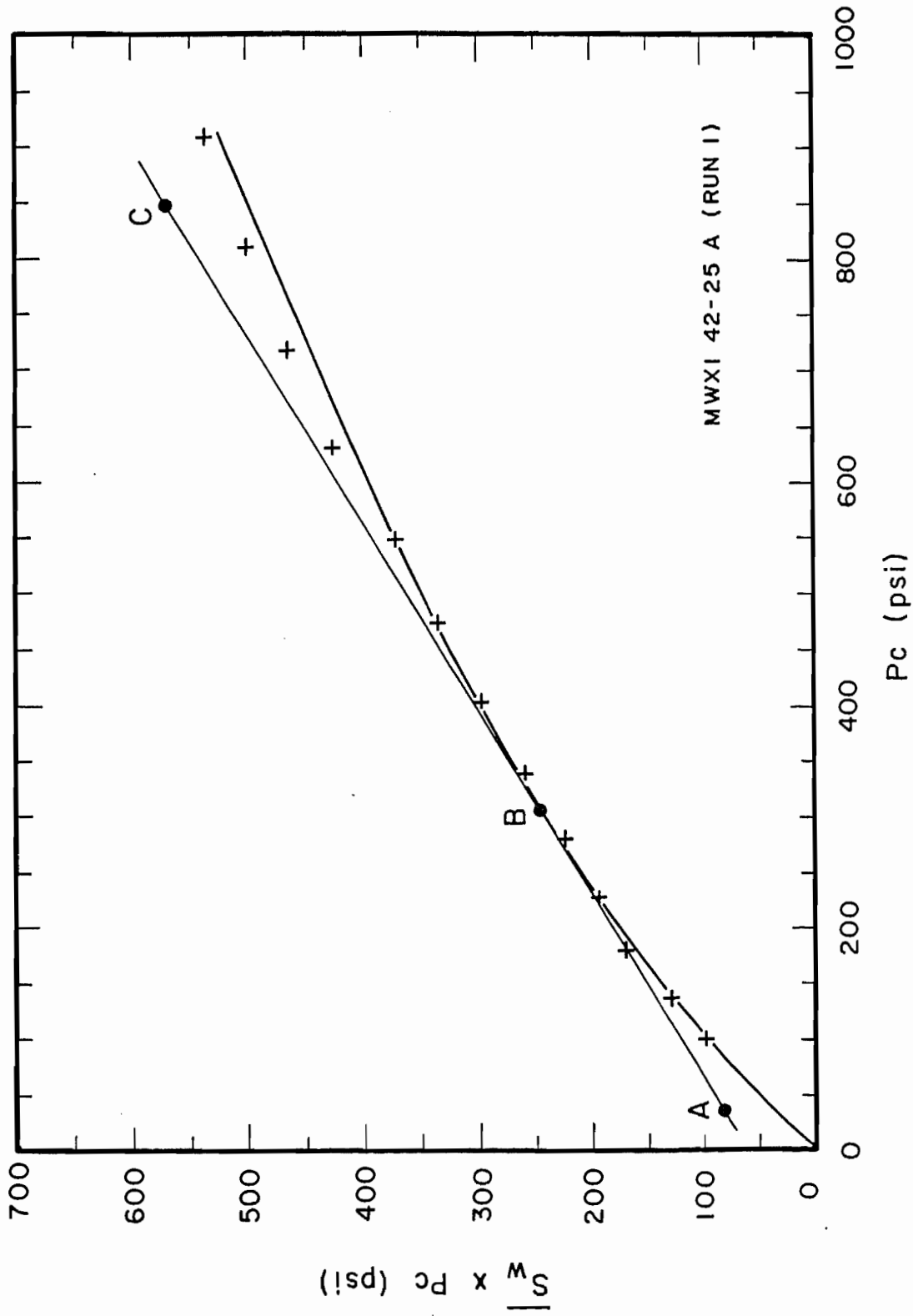


Figure 5. Graphical interpretation of centrifuge data - Method 1.

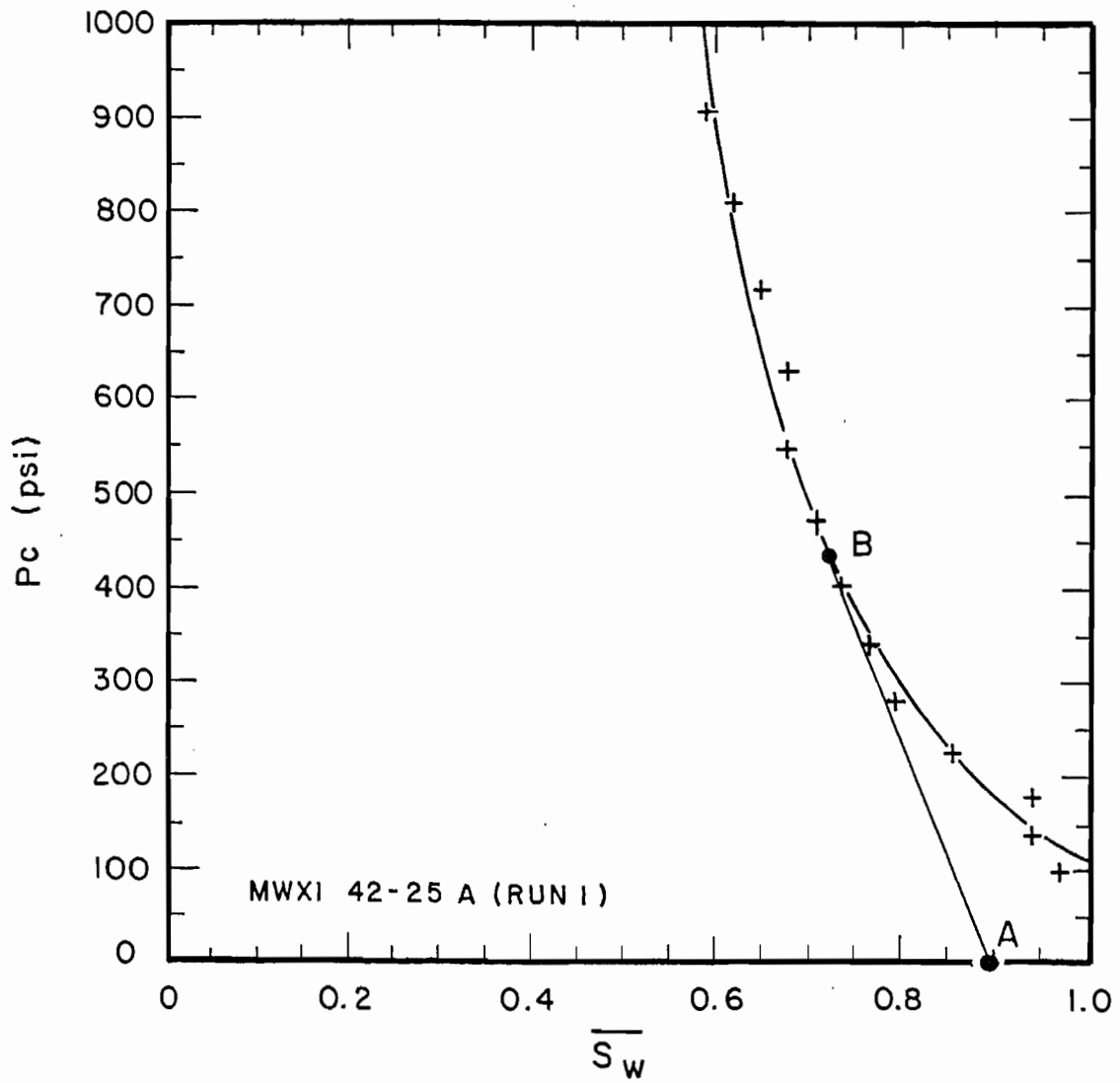


Figure 6. Graphical interpretation of centrifuge data - Method 2.

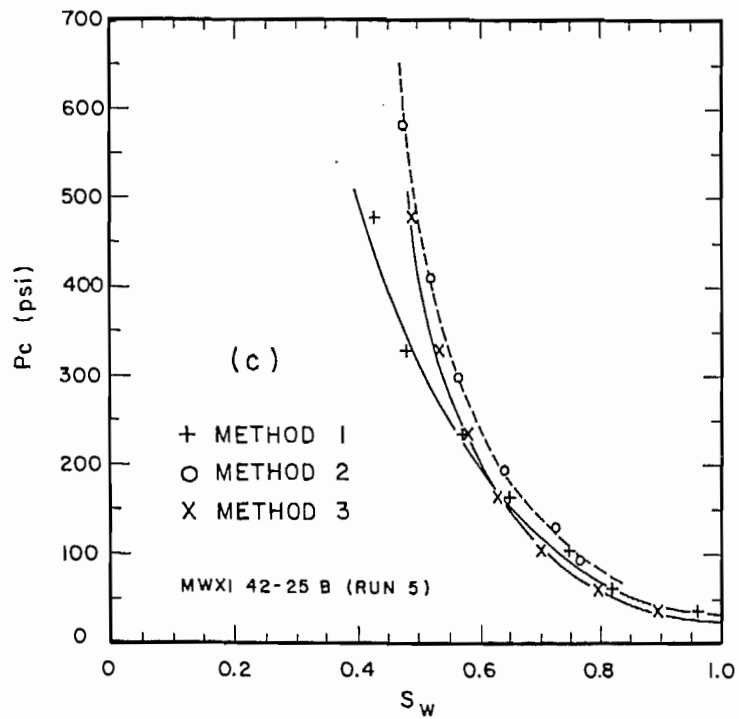
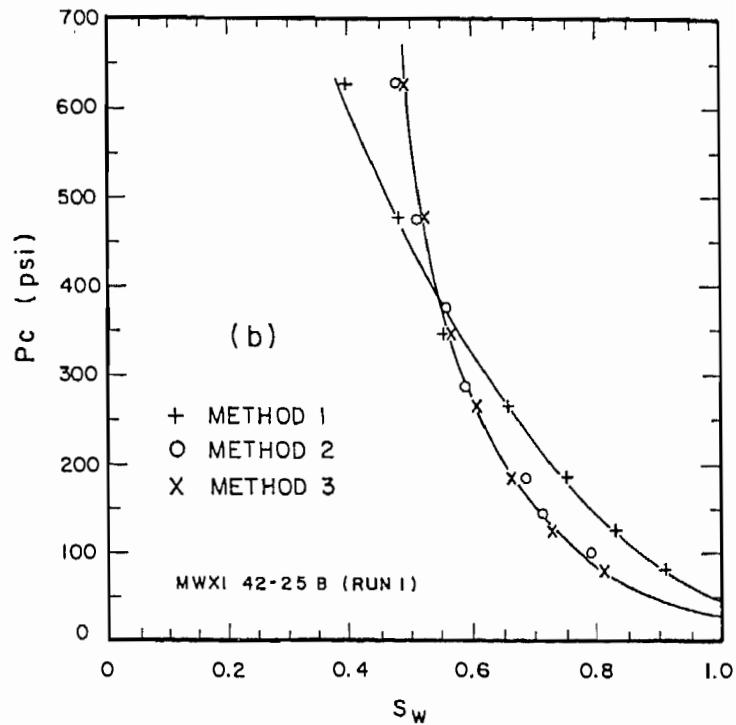
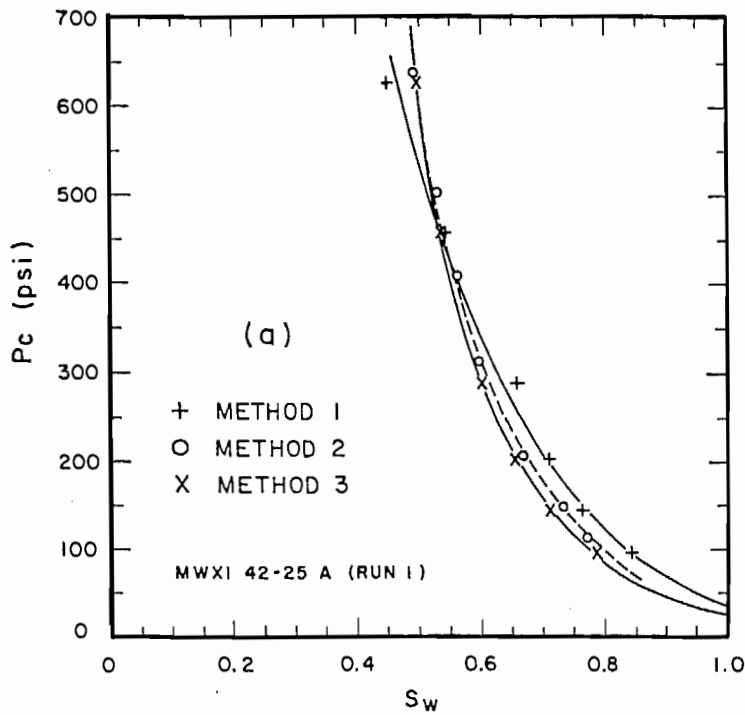


Figure 7. Comparisons of capillary pressure curves calculated by Methods 1, 2 and 3.

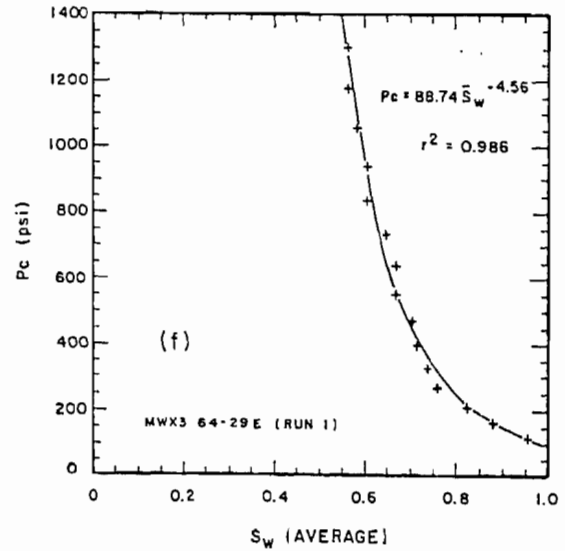
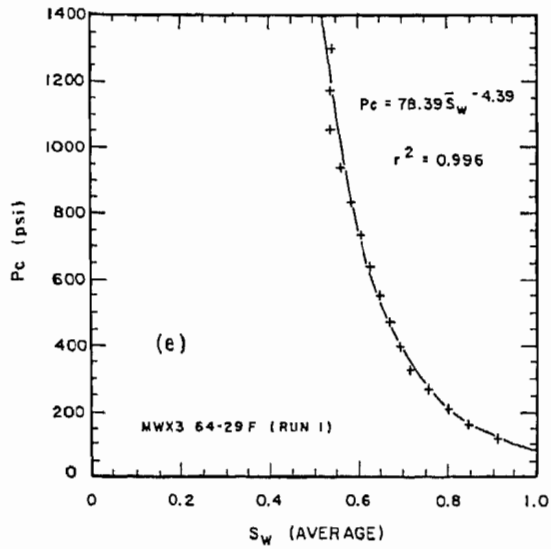
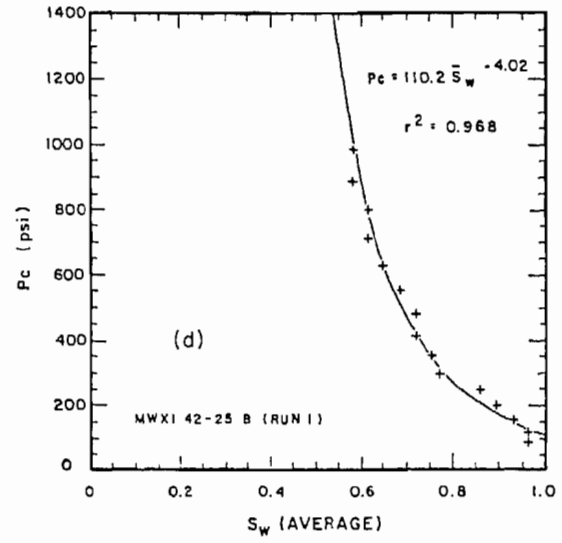
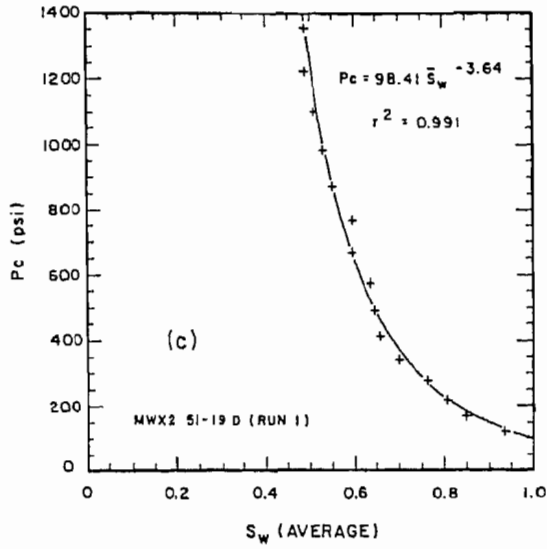
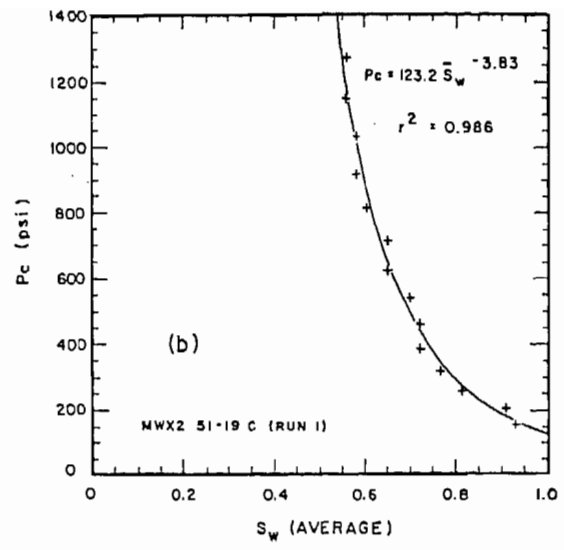
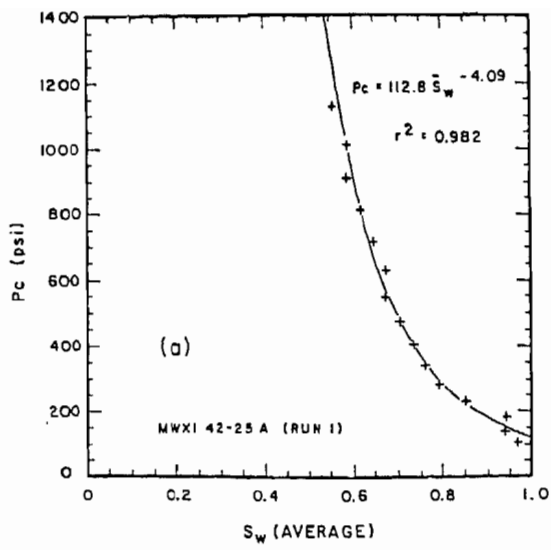


Figure 8. Least-squares fits to Multiwell centrifuge data - Run 1, air displacing brine.

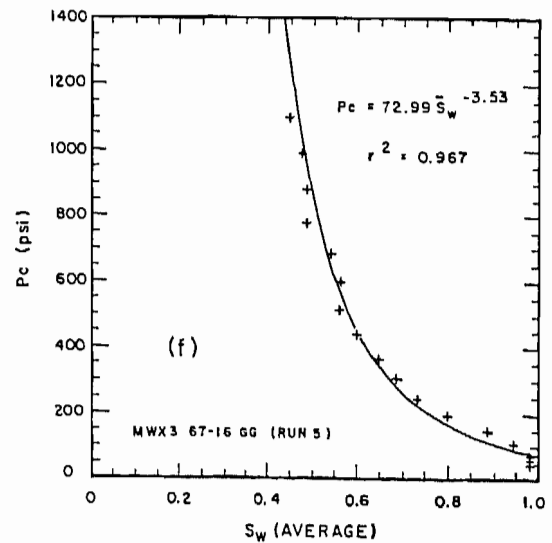
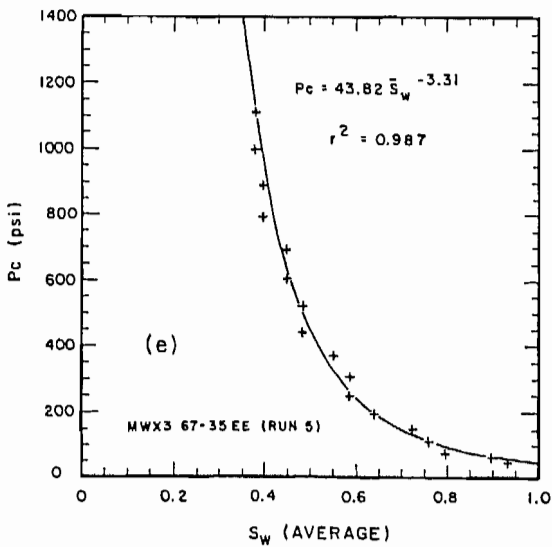
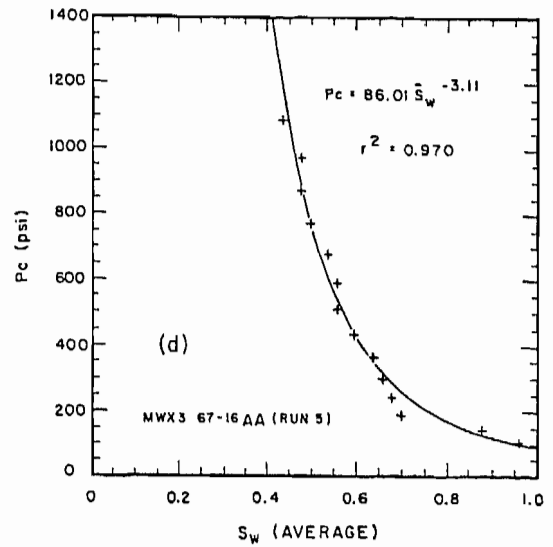
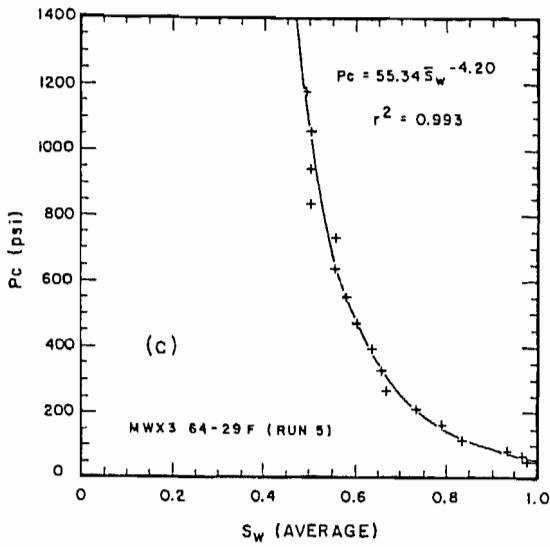
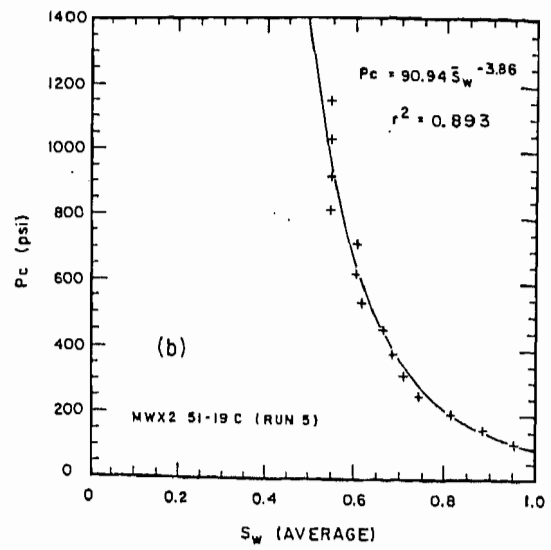
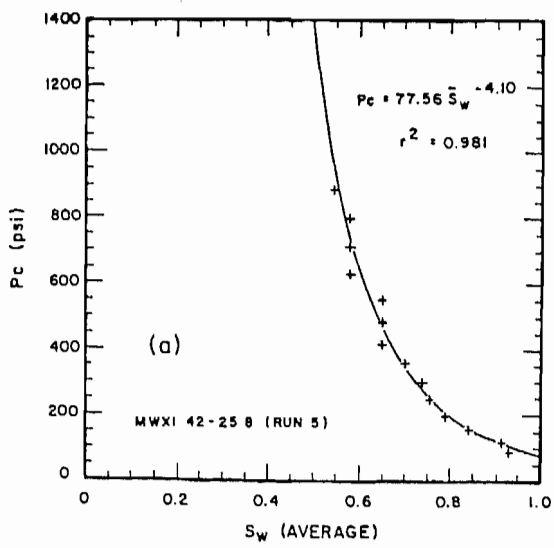


Figure 9. Least-squares fits to Multiwell centrifuge data - Run 5, air displacing brine.

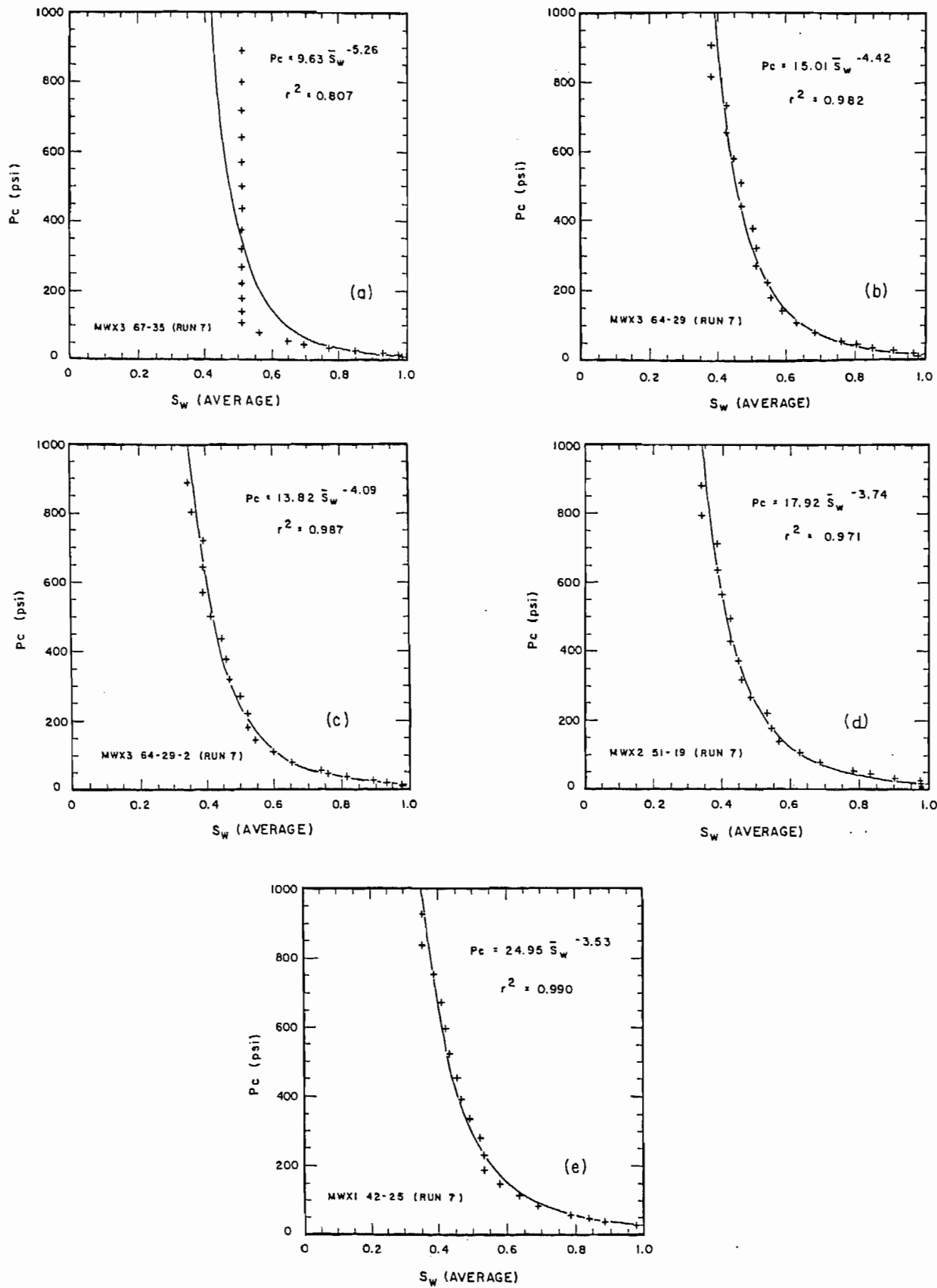


Figure 10. Least-squares fits to Multiwell centrifuge data - Run 7, air displacing decane.

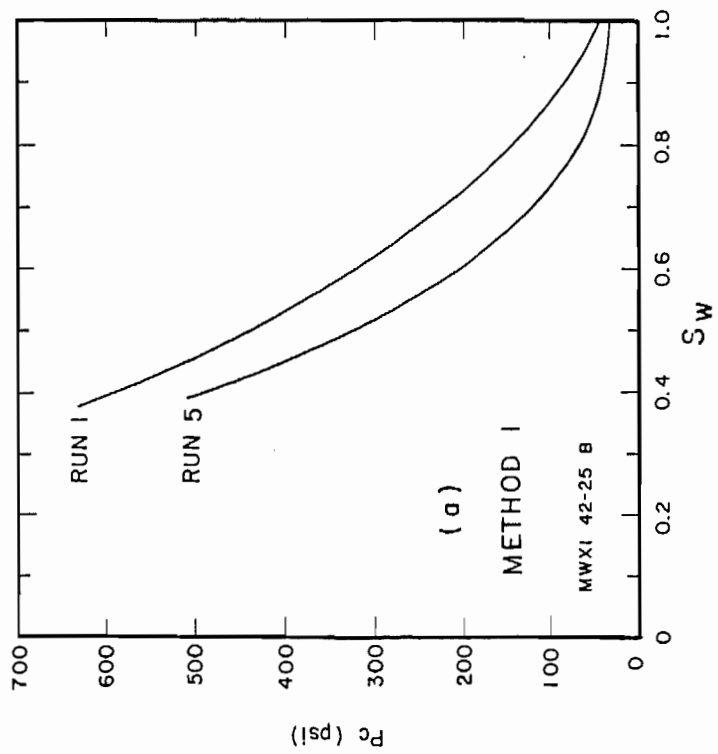
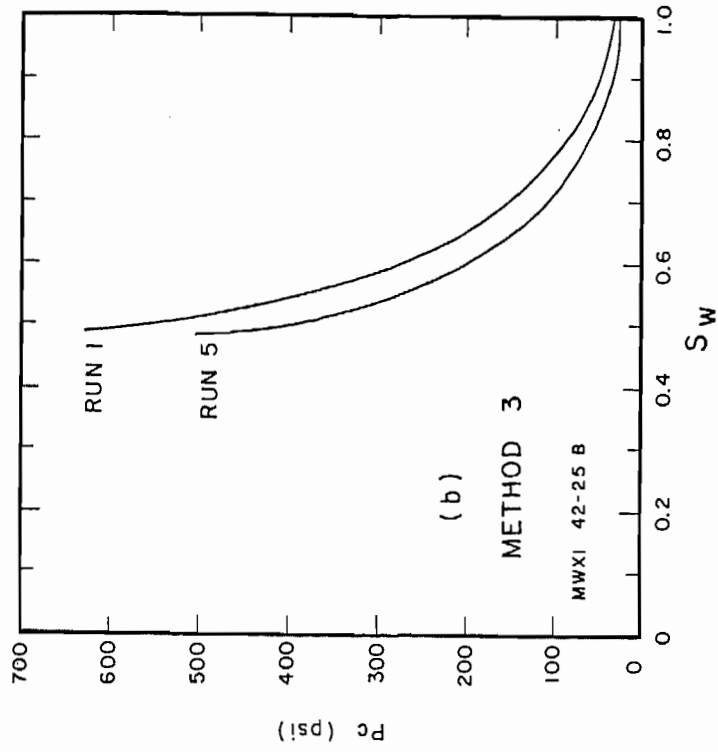


Figure 11. Reproducibility of capillary pressure curves calculated by methods 1 and 3.